Chinese Journal of Catalysis 39 (2018) 1511–1519

available at www.sciencedirect.com

ScienceDirect

journal homepage: www.elsevier.com/locate/chnjc

Article

Silicoaluminophosphate molecular sieve DNL-6: Synthesis with a novel template, *N,N*'-dimethylethylenediamine, and its catalytic application

Pengfei Wu [a,b], Miao Yang [a], Wenna Zhang [a,b], Shu Zeng [a,b], Mingbin Gao [a,b], Shutao Xu [a], Peng Tian [a,*], Zhongmin Liu [a,#]

[a] *National Engineering Laboratory for Methanol to Olefins, Dalian Institute of Chemical Physics, Chinese Academy of Sciences, Dalian 116023, Liaoning, China*

[b] *University of Chinese Academy of Sciences, Beijing 100049, China*

ARTICLE INFO

Article history:
Received 7 May 2018
Accepted 2 June 2018
Published 5 September 2018

Keywords:
N,N'-dimethylethylenediamine
SAPO molecular sieves
Synthesis
DNL-6
Methanol amination reaction

ABSTRACT

DNL-6, a silicoaluminophosphate (SAPO) molecular sieve with RHO topology, was hydrothermally synthesized using a new structure-directing agent (SDA), *N,N*'-dimethylethylenediamine. The obtained samples were characterized by X-ray diffraction, X-ray fluorescence, X-ray photoelectron spectroscopy, scanning electron microscopy, and N_2 adsorption, which indicated that the synthesized DNL-6s have high crystallinity and relatively high Si content ranging from 20% to 35%. Solid-state magic-angle-spinning (MAS) nuclear magnetic resonance (^{13}C, ^{29}Si, ^{27}Al, ^{31}P, and ^{27}Al multiple-quantum (MQ)) was conducted to investigate the status of the SDA and local atomic environment in the as-synthesized DNL-6. Thermal analysis revealed the presence of a large amount of amines in the DNL-6 crystals (about 4.4 SDAs per α-cage), which was the reason for the formation of DNL-6 with an ultrahigh Si content (36.4% Si per mole). Interestingly, DNL-6 exhibited excellent catalytic performance for methanol amination. More than 88% methanol conversion and 85% methylamine plus dimethylamine selectivity could be achieved due to the combined contribution of strong acid sites, suitable acid distribution, and narrow pore dimensions of DNL-6.

1. Introduction

Silicoaluminophosphate (SAPO) molecular sieves, first reported by the Union Carbide Corporation in the 1980s, are important microporous materials often used in industrial catalytic processes [1–4]. The incorporation of Si atoms into neutral aluminophosphate frameworks results in a moderate acidity and high thermal and hydrothermal stabilities, which make them suitable for many important applications. For example, SAPO-34 with a CHA structure is an excellent catalyst for the methanol-to-olefin (MTO) reaction [5,6] and its Cu^{2+} ion-exchanged counterpart shows a superior catalytic performance and stability for the selective catalytic reduction (SCR) of NO_x [7,8]. Further, Pt/SAPO-11 was used as a catalyst for hydro-isomerization due to its outstanding isomerization activity and lower cracking activity [9,10].

The impressive properties and consequent important applications of SAPO molecular sieves are mainly controlled by

* Corresponding author. Tel: +86-411-84379218; Fax: +86-411-84691570; E-mail: tianpeng@dicp.ac.cn
# Corresponding author. Tel: +86-411-84379998; Fax: +86-411-84691570; E-mail: liuzm@dicp.ac.cn
This work was supported by the National Natural Science Foundation of China (21476228, 21676262) and the Key Research Program of Frontier Sciences, CAS (QYZDB-SSW-JSC040).
DOI: 10.1016/S1872-2067(18)63122-5 | http://www.sciencedirect.com/science/journal/18722067 | Chin. J. Catal., Vol. 39, No. 9, September 2018

their Si distribution and morphology. Considerable efforts have been put in over the past few decades to develop synthetic strategies for SAPO molecular sieves. Generally, the synthesis of SAPO molecular sieves is influenced by a number of parameters, such as the type of initial sources, solvent, crystallization temperature, and time. The structure-directing agent (SDA) is one of the most important factors; it plays complicated roles in the synthesis process, such as dissolving the raw materials, orienting the structure, balancing the charges, and filling the skeleton space [11]. Consequently, the crystalline phase, morphology, composition, and acidity of the final SAPO products can be modified by template selection. Taking the synthesis of SAPO-34 as an example, low silicon SAPO-34 can only be synthesized using a large organic amine template, such as trimethylamine (TEA) or tetraethylammonium hydroxide (TEAOH), because only one protonated template molecule can be accommodated in one CHA cage to balance the negative charge of the framework. Meanwhile, SAPO-34s synthesized by small organic amines, such as diethylamine (DEA), piperazine (PIP), and morpholine (MOR), have relatively high Si contents due to their small volume and high charge density [12–14]. More interestingly, the SAPO-34 product directed by TEAOH presents a nano-sized morphology, which exhibits an improved MTO catalytic performance. The strong alkalinity of TEAOH may induce the dissolution of the silica source, which promotes nucleation and small-crystal formation [15,16]. Hence, discovering novel SDAs is an effective way to modify the properties of SAPO molecular sieves.

DNL-6 is an SAPO molecular sieve with an RHO topology (composed of α-cages linked via double 8-rings), which was first reported by our laboratory. It was found accidentally during an investigation on the phase-transformation processes of SAPO molecular sieves [17]. Thereafter, the synthesis of DNL-6 was accomplished by various strategies including surfactant-assisted hydrothermal synthesis [18], dry-gel conversion [19], and aminothermal crystallization [20]. It is noteworthy that DNL-6 possesses strong Brønsted acid sites comparable to those of HZSM-5 or even stronger [21], over which heptamethylbenzenium cations (heptaMB$^+$) were stabilized and directly observed for the first time during a real MTO reaction [22]. Moreover, the material can accommodate high concentrations of single Si(OAl)$_4$ species, indicating huge potential for CO_2/CH_4 and CO_2/N_2 adsorption/separation [19]. Optimized synthesis of DNL-6 is thus highly desired; it may provide opportunities to develop new applications.

Thus far, diethylamine (DEA) is the only known template to synthesize DNL-6. Moreover, the use of cationic surfactants is important for the synthesis of DNL-6. The strong adsorption of cationic surfactant molecules on SAPO species protects DNL-6 from dissolving, and inhibits its transformation to SAPO-34 [23]. In this work, we report a new template, *N,N*'-dimethylethylenediamine, to synthesize DNL-6 molecular sieves. Notably, a cationic surfactant is not necessary anymore. The synthesized DNL-6s were characterized by various techniques including X-ray diffraction (XRD), X-ray fluorescence (XRF), X-ray photoelectron spectroscopy (XPS), scanning electron microscopy (SEM), N_2 adsorption, and solid-state magic-angle spinning nuclear magnetic resonance (solid-state MAS NMR). The sample with an ultrahigh silica content and acidity shows excellent catalytic activity and a remarkable methylamine and dimethylamine selectivity in the methanol amination reaction.

2. Experimental

2.1. Sample preparation

A typical hydrothermal synthesis procedure for DNL-6 is as follows. Orthophosphoric acid (85 wt%) and tetraethyl orthosilicate were mixed with a solution of aluminum isopropoxide and deionized water. After the synthesis solution was stirred for 2 h, the template agent, *N,N*'-dimethylethylenediamine, was added and it was continually stirred for 4 h. Later, the synthesis gel was transferred into a stainless steel autoclave and heated at 200 °C for 12 h under rotation. After equilibrating for a certain time period at this temperature for crystallization, the autoclave was cooled down and the solid product was recovered by filtration, washed three times with deionized water, and dried at 110 °C overnight. Finally, the product was calcined at 550 °C for 4 h to remove organic species.

2.2. Characterization

Powder XRD patterns were recorded on a PANalytical X'Pert PRO X-ray diffractometer with Cu K_α radiation (λ = 1.54059 Å), operating at 40 kV and 40 mA. SEM images were generated on a Hitachi SU8020 electron microscope at 25 kV. The bulk and surface compositions of samples were determined using a Philips Magix-601 XRF spectrometer and a VG ESCALAB MkII XPS. N_2 adsorption measurements were carried out on a Micromeritics 2010 analyzer at –196 °C after the sample was degassed at 350 °C under vacuum. All solid-state NMR experiments were performed on a Bruker Avance III 600 spectrometer equipped with a 14.1 T wide-bore magnet and a 4 mm MAS probe. The resonance frequencies at this field strength were 150.9, 156.4, 119.2, and 242.9 MHz for ^{13}C, ^{27}Al, ^{29}Si, and ^{31}P, respectively. ^{13}C cross polarization (CP)/MAS NMR spectra were recorded with a contact time of 3 ms and recycle delay of 2 s at a spinning rate of 12 kHz. ^{27}Al MAS NMR spectra were recorded using one pulse sequence at a spinning rate of 12 kHz. A total of 200 scans were accumulated with a π/8 pulse width of 0.75 μs and a 2 s recycle delay. Chemical shifts were referenced to $(NH_4)Al(SO_4)_2{\cdot}12H_2O$ at –0.4 ppm. ^{29}Si and ^{31}P MAS NMR spectra were recorded by high-power proton decoupling. ^{29}Si MAS NMR spectra were recorded with a π/4 pulse width of 2.5 μs and a recycle delay of 10 s at a spinning rate of 8 kHz. Chemical shifts were referenced to kaolinite at –91.5 ppm. ^{31}P MAS NMR spectra were recorded with a π/4 pulse width of 2.25 μs and a 10 s recycle delay. Chemical shifts were referenced to 85% H_3PO_4 at 0 ppm. Two-dimensional (2D) ^{27}Al multiple quantum magic angle spinning (MQ-MAS) NMR analysis was performed on a 4 mm H-X WVT probe at a spinning rate of 13 kHz. An rf field of 49.1 kHz was used for the creation (0Q → ±3Q) and first conversion (±3Q → 0Q) pulses. The central tran-

sition selective soft 90° pulse used for the last conversion step (0Q → ±1Q) was 3.47 kHz. A shearing transformation was used to achieve 2D Fourier transformation and obtain a pure absorption-mode 2D contour plot. The quadrupolar interaction product, P_Q (P_Q is identical to the "second order quadrupole effect (SOQE)" parameter used in various publications), and isotropic chemical shift (δ_{iso}) values were calculated according to procedures reported previously [24]. The ^{1}H MAS NMR spectra were recorded using a 4 mm MAS probe. The pulse width was 2.2 μs for a π/4 pulse and 32 scans were accumulated with a 4 s recycle delay. The samples were spun at 12 kHz and chemical shifts were referenced to adamantine at 1.74 ppm. Thermogravimetric analyses (TG-DTG) were performed on a TA Q600 analyzer. The sample was heated at a rate of 10 °C/min to 900 °C. Temperature-programmed desorption by NH_3 (NH_3-TPD) experiments were conducted on an automated characterization system (AutoChem 2920, Micromeritics) with a TCD detector. The calcined sample (200 mg) was compressed into pellets (40–60 mesh) and packed into a U-tube reactor. The packed column was initially purged with He flow and outgassed at 600 °C. After pretreatment, the sample was cooled to 100 °C and saturated with ammonia. Physically adsorbed ammonia was swept by purging with He at a flow rate of 40 mL/min for 30 min. Finally, the packed bed was heated at a rate of 10 °C/min to 600 °C under He flow (20 mL/min).

2.3. Catalytic test

Methanol amination experiments were performed in a continuous flow fixed-bed reactor at atmospheric pressure. A 0.3 g portion of the calcined sample (40–60 mesh) was loaded into the reactor and pretreated in He (40 mL/min) at 500 °C for 1 h prior to the reaction. The temperature of the catalyst bed was cooled to reaction temperature (260 or 300 °C) in He. A NH_3 flow of 6.2 mL/min was fed into the reactor by a mass-flow controller. Methanol was introduced into the system by passing He (47 mL/min) through a methanol-filled saturator (10 °C), which resulted in a weight hourly space velocity (WHSV) of 0.813 h^{-1} and methanol/ammonia = 0.5 (mole). The products were analyzed on-line using an Agilent 6890 gas chromatograph with a flame ionization detector (FID) using a CP-Volamine column.

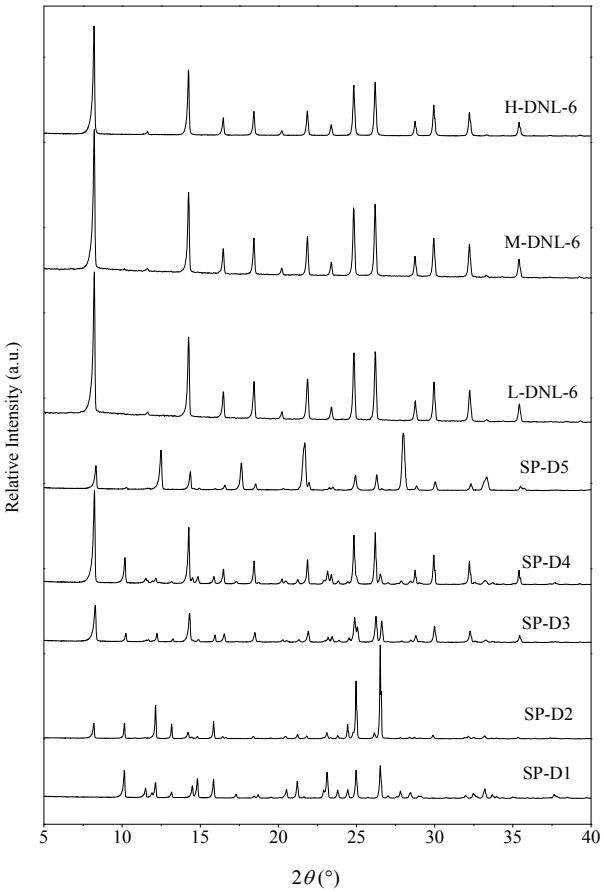

Fig. 1. XRD patterns of the as-synthesized samples.

3. Results and discussion

3.1. Synthesis and characterization of DNL-6

The detailed synthesis conditions including gel composition, crystallization time, product crystalline phases, and composition are listed in Table 1. The corresponding XRD patterns of these products are shown in Fig. 1. When TEOS is absent (SP-D1), $AlPO_4$-21 with an AWO topology is the final product. The AWO phase decreases and RHO phase increases with an

Table 1
Gel compositions and resultant products of hydrothermal syntheses.

Sample [a]	Gel composition $TEOS/Al_2O_3/P_2O_5/R/H_2O$	Crystalline phase	Product composition	
			Bulk (XRF)	Surface (XPS)
SP-D1	0 /1.0/1.0/5.0/167.0	AWO	–	–
SP-D2	0.3 /1.0/1.0/5.0/167.0	AWO + RHO	–	–
SP-D3	0.6 /1.0/1.0/5.0/167.0	RHO + AWO	–	–
L-DNL-6	1.3/1.3/1.0/5.0/167.0	RHO	$Si_{0.226}Al_{0.475}P_{0.230}O_2$	$Si_{0.262}Al_{0.292}P_{0.446}O_2$
M-DNL-6	1.2/1.0/1.0/5.0/167.0	RHO	$Si_{0.286}Al_{0.454}P_{0.259}O_2$	$Si_{0.346}Al_{0.421}P_{0.233}O_2$
H-DNL-6	1.7/1.0/1.0/5.0/167.0	RHO	$Si_{0.364}Al_{0.414}P_{0.222}O_2$	$Si_{0.462}Al_{0.377}P_{0.161}O_2$
SP-D4 [b]	1.2/1.0/1.0/5.0/167.0	RHO + GIS	$Si_{0.231}Al_{0.464}P_{0.305}O_2$	–
SP-D5 [b]	1.2/1.0/1.0/5.0/167.0	GIS + minor RHO	$Si_{0.252}Al_{0.466}P_{0.282}O_2$	–

[a] The crystallization conditions are 200 °C and 12h. [b] The crystallization time is 68 h for SP-D4 and 143 h for SP-D5.

increase in the amount of TEOS. Pure DNL-6 molecular sieves cannot be synthesized unless the molar ratio of TEOS/Al_2O_3 is 1. Further, an amorphous phase appears along with DNL-6 when the TEOS/Al_2O_3 molar ratio is greater than 1.7. Pure-phase DNL-6s synthesized at TEOS/Al_2O_3 ratios of 1.0, 1.2, and 1.7 were denoted as L-DNL-6, M-DNL-6, and H-DNL-6, respectively. Their Si contents range from 22.4% to 36.4%. It should be noted that SAPO molecular sieves with such high Si contents are rarely reported. Upon further prolonging the crystallization time, the RHO phase gradually converts to a dense GIS phase (68 h for SP-D4 and 143 h for SP-D5), indicating the metastable characteristics of DNL-6. Meanwhile, the Si content of solid products is higher than that of M-DNL-6.

All pure DNL-6 samples are present in the form of micron-sized particles, as shown in Fig. 2. The product morphology changes with an increase in the Si content; L-DNL-6 is sphere-like (Fig. 2(a) and (b)) and M-DNL-6 exhibits a truncated rhombic dodecahedron morphology (Fig. 2(c) and (d)). H-DNL-6 exhibits a spherical morphology with an average particle size of about 4 μm, whose outer layer consists of small cubic crystals of 50 nm size (Fig. 2(e) and (f)).

The textural properties of the obtained DNL-6 samples were characterized by N_2 adsorption and are shown in Fig. 3 and Table 2. The samples exhibit Type I adsorption-desorption isotherms with little mesopore volume, indicating that the inner regions of the particles are solid. All DNL-6 samples exhibit large Brunauer-Emmett-Teller (BET) micropore surface area and volume, which verifies their high crystallinity. In particular, owing to the rough surfaces of the particles, the external surface area of H-DNL-6 is larger than that of its analogs.

The chemical environments of the as-synthesized DNL-6s were analyzed by solid-state MAS NMR, as shown in Fig. 4. The ^{13}C/CP MAS NMR spectra (Fig. 4(a)) show two strong resonance peaks at 44.1 and 32.9 ppm, corresponding to the methylene and methyl groups of *N,N'*-dimethylethylenediamine template, respectively. The two weak split signals at about 55 ppm are caused by strong interactions between the methylene groups of templates and the molecular sieve framework [25,26]. These results verify the intact status of the organic amine in the synthesized DNL-6 crystals. Fig. 4(b) displays the ^{27}Al NMR spectra of the samples, all of which show a broad peak at 39 ppm; it can be assigned to the tetrahedrally coordinated Al species of the framework. The ^{31}P NMR spectra (Fig. 4(c)) show a peak at –29 ppm attributable to the tetrahedral PO_4 group. The ^{29}Si NMR spectra become complicated with increasing Si content in DNL-6, as shown in Fig. 4(d). L-DNL-6 shows a strong signal at –92 ppm and a very weak peak at –95 ppm indicating that Si(4Al) is the main environment for L-DNL-6. Meanwhile, M-DNL-6 shows quadruple signals at –92, –95, –99, and –104 ppm, indicating the appearance of a large number of Si(3Al), Si(2Al) and Si(1Al) species. Regarding H-DNL-6, a quintuplet of signals appears at –92, –95, –99, –104, and –109 ppm. The signals at –95, –99, and –104 ppm are as strong as the signal at –92 ppm, suggesting that the amount of Si(3Al), Si(2Al), and Si(1Al) increased. In addition, the chemical shift at –109 ppm indicates the existence of Si islands. The surface compositions of DNL-6 products were evaluated by XPS, as shown in Table 1. As expected, all the DNL-6 samples contain high Si contents on the crystal surface [27]. As the degree of Si enrichment increases, the surface P and Al contents show a corresponding decrease. Combining the XPS results and ^{29}Si NMR spectra, it is believed that the outer surfaces of DNL-6

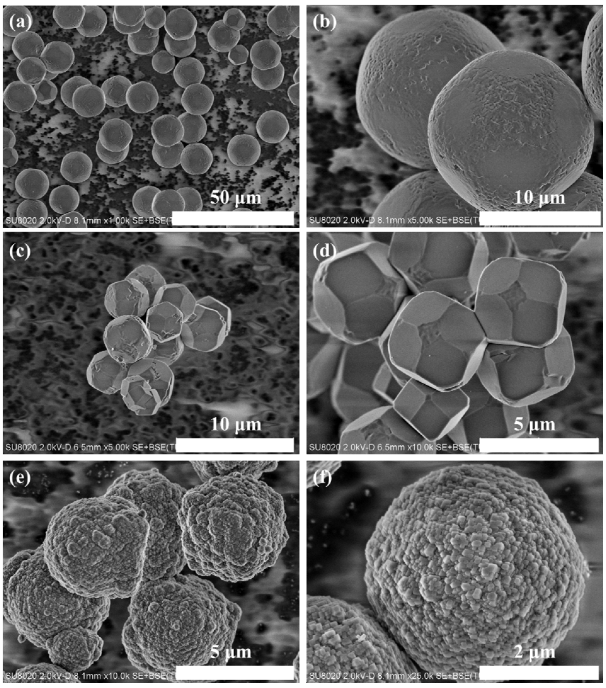

Fig. 2. SEM images of calcined L-DNL-6 (a, b), M-DNL-6 (c, d), and H-DNL-6 (e, f).

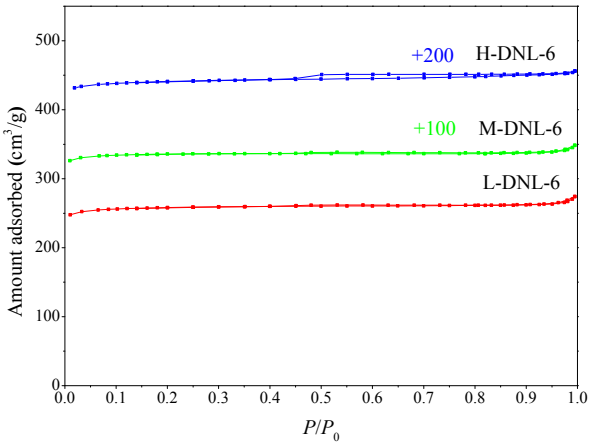

Fig. 3. N_2 sorption isotherms of DNL-6 samples.

Table 2
Textural properties of the samples.

Sample	S_{BET} [a] (m^2/g)	S_{mic} [b] (m^2/g)	S_{ext} [b] (m^2/g)	V_{mic} [b] (cm^3/g)	V_{meso} [c] (cm^3/g)
L-DNL-6	817	772	45	0.38	0.04
M-DNL-6	745	711	34	0.35	0.03
H-DNL-6	854	794	60	0.37	0.03

[a] Total surface area is determined by the BET equation. [b] Micropore surface area, external surface area, and volume are determined by the t-plot method. [c] Mesopore volume is determined from the adsorption isotherms by the BJH method.

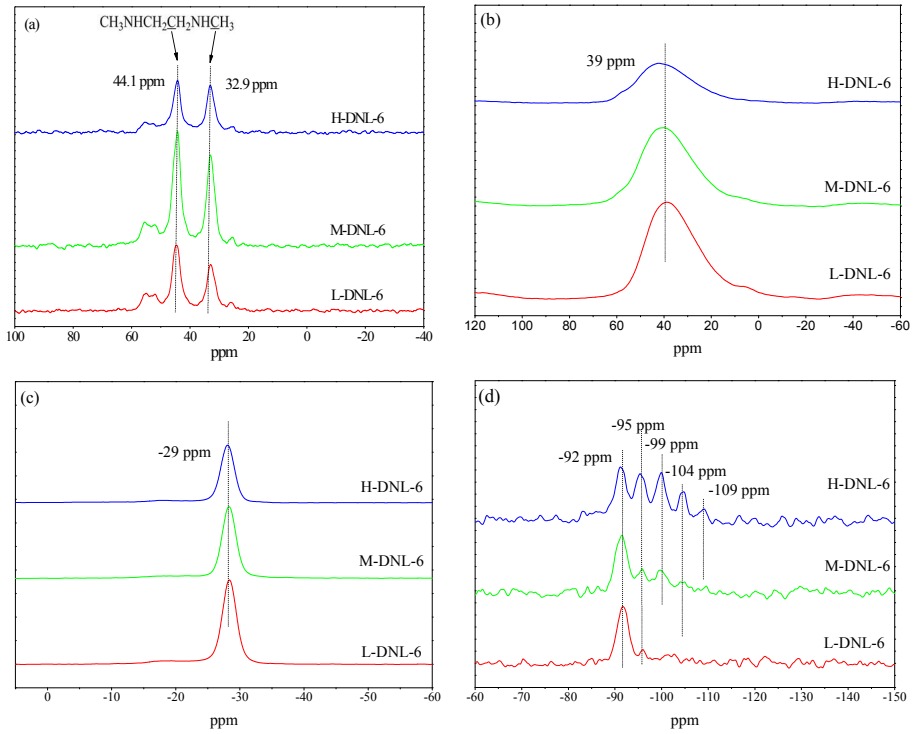

Fig. 4. ^{13}C (a), ^{27}Al (b), ^{31}P (c), and ^{29}Si (d) MAS NMR spectra of the as-synthesized samples.

crystals have more complex Si environments (more Si islands) than the inner parts.

In order to further understand the atomic chemical environment of H-DNL-6, ^{27}Al MQ-MAS NMR analysis was conducted on calcined H-DNL-6 because Al atoms are the bridges for Si and P atoms. As ^{27}Al is a quadrupolar nucleus, the single-pulse MAS NMR spectral line shape is often markedly broadened, owing to residual second-order quadrupolar interactions. ^{27}Al MQ-MAS NMR can effectively eliminate the second-order quadrupolar interactions experienced by half-integer quadrupolar nuclei and thus narrow down asymmetric line shapes considerably [28]. The ^{27}Al MQ-MAS NMR spectrum of calcined H-DNL-6 is shown in Fig. 5. The indirect dimension (F1) displays five peaks at 34, 42, 48, 59, and 67 ppm, which are preliminarily attributed to $Al(OP)_4$ (IV_a), $Al(OSi)_n(OP)_{(4-n)}$ (n = 1, 2, and 3) (IV_b and IV_c), and $Al(OSi)_4$ (IV_d and IV_e), respectively [21,29]. The peak at 42 ppm is the strongest, showing that $Al(OSi)_n(OP)_{(4-n)}$ (n = 1, 2, and 3) corresponding to Si atoms at the borders of Si islands, is a dominant chemical environment in H-DNL-6. On the basis of these results, the distributions of Si concentration and Si environments in the H-DNL-6 crystals are proposed and illustrated in Fig. 6. Si content increases gradually from the inner part to the exterior part of the crystals. The shell region of the crystals is enriched with large Si islands and the region adjacent to the shell contains a number of relatively small Si islands, both of which provide Si(nAl) (n = 1, 2, and 3) environments. The interior of H-DNL-6 crystals, which has a relatively low Si content, is enriched with Si(4Al) species.

Thermal analysis was carried out to investigate the content

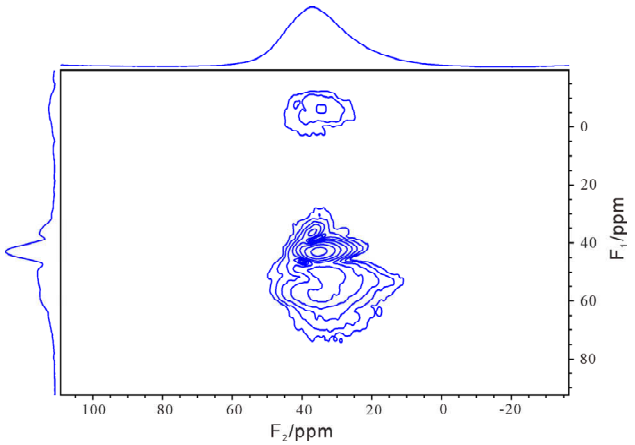

Fig. 5. ^{27}Al MQ-MAS NMR spectrum of calcined H-DNL-6.

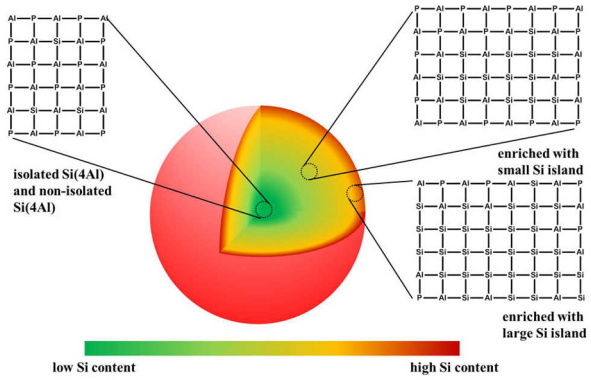

Fig. 6. The distribution of Si concentration and Si environments in a H-DNL-6 crystal.

and existing status of the *N,N*'-dimethylethylenediamine template. The TG curves are shown in Fig. 7. The first weight loss stage of ca. 5 wt % from room temperature to 200 °C corresponds to the desorption of physically adsorbed water. The second weight loss of around 20 wt % between 200 and 800 °C could be attributed to the decomposition of the template molecules occluded within the crystals. The detailed weight loss data of the three DNL-6 samples are listed in Table 3. The number of *N,N*'-dimethylethylenediamine molecules per α cage is calculated to be about 4.4, very similar to that of DNL-6 directed by DEA (4.28 DEA per α cage) [18]. However, *N,N*'-dimethylethylenediamine has an obviously higher charge density than DEA due to its low C/N ratio (2:1 vs. 4:1). This means that it is possible for one *N,N*'-dimethylethylenediamine molecule to carry double positive charges, which can balance more negative charges induced by greater Si incorporation. This result is consistent with the high Si concentration of DNL-6 samples.

3.2. Catalytic performance

Methylamines, especially methylamine (MMA) and dimethylamine (DMA), are important industrial chemicals for producing pesticides, pharmaceuticals, surfactants, and solvents. Up to now, almost all methylamines are being produced by the reaction of methanol and ammonia on an amorphous silica-alumina-based catalyst [31]. The synthesis route of methylamines from methanol and ammonia is illustrated in Scheme 1. It is mentioned that dimethyl ether, obtained by the dehydration of methanol, can undergo the same reaction as methanol with NH_3, MMA, and DMA to produce methylamines [31].

One marked drawback of current industrial catalysts is that

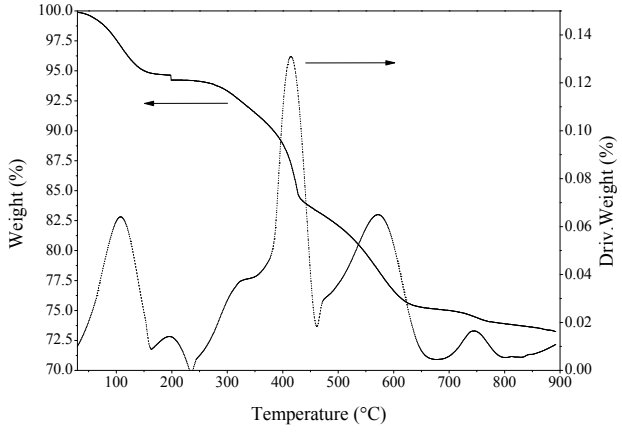

Fig. 7. TG-DTG curves of as-synthesized M-DNL-6.

Table 3
Thermal properties of the samples.

Sample	Weight loss (%)		Moles of water per cage	Moles of R per cage
	RT–200 °C	200–800 °C		
H-DNL-6	4.80	20.23	5.14	4.42
M-DNL-6	5.76	20.34	6.27	4.51
L-DNL-6	5.12	20.10	5.32	4.27

$$CH_3OH + NH_3 \longrightarrow \begin{matrix} CH_3NH_2\ (MMA) \\ (CH_3)_2NH\ (DMA) \\ (CH_3)_3N\ (TMA) \end{matrix}$$

Scheme 1. Synthesis of methylamines from methanol and ammonia.

the product distribution of the reaction obeys a thermodynamic equilibrium, producing trimethylamine (TMA) predominantly instead of MMA and DMA. Thus, small-pore molecular sieve catalysts, such as RUB-1 [32], RHO, SSZ-16, and SAPO-34 [33,34], have been investigated in order to optimize reaction selectivity and meet commercial demands. The lack of strong acid sites is one of the main drawbacks hindering the application of SAPO materials as amination catalysts, resulting in a lower methanol conversion and much higher selectivity for dimethyl ether than the corresponding aluminosilicate analogs [33]. According to literature, DNL-6 possesses very strong Brønsted acid sites, similar to the aluminosilicate HZSM-5. Moreover, the pore dimensions of DNL-6 (3.6 × 3.6 Å) are smaller than the shortest dimension of TMA (3.9 Å), which may help to suppress the formation of bulk TMA.

The catalytic performance of DNL-6 samples was evaluated in the methanol amination reaction at reaction temperatures of 260 and 300 °C, methanol WHSV of 0.813 h^{-1}, and *n*(ammonia):*n*(methanol) = 2:1. The steady-state catalytic results are illustrated in Table 4. The main products are MMA and DMA with all DNL-6 catalysts. Increasing the reaction temperature from 260 to 300 °C could greatly improve the catalytic activity. However, the selectivity for MMA decreased obviously accompanied by an increase in DMA and TMA, due to an enhanced methylation reaction at elevated temperatures. H-DNL-6, with its ultrahigh silica content, induces the highest methanol conversion and selectivity for MMA plus DMA. Fig. 8 illustrates the changes in methanol conversion and product selectivity with time on stream for H-DNL-6 at 300 °C. It is clear that the reaction is stable during the investigated period; further, methanol conversion is higher than 88% and selectivity for MMA plus DMA is greater than 85%.

Considering that acidity plays an important role in the methanol amination reaction [33], NH_3-TPD was conducted to investigate the acidity of DNL-6 samples in order to better understand the catalytic results. As shown in Fig. 9, there are two desorption peaks corresponding to NH_3 desorbed from weak and strong acid sites. All the samples exhibit similar acid strength, despite the different acid concentrations. A gradual drop in strong acid sites can be observed following an increase in Si concentration in the samples. Moreover, H-DNL-6 possesses a small amount of super-strong acid sites (the corresponding desorption temperature is higher than 550 °C), which are absent in L-DNL-6 and M-DNL-6. Because the acidity of different Si environments in SAPO molecular sieves follows the order of Si(1Al) > Si(2Al) > Si(3Al) > Si(4Al), it is speculated that the super-strong acid sites are located at the borders of larger Si islands in H-DNL-6 [6]. These acid characterization results suggest that acid strength is more important than acid density for the methanol amination reaction activity. Furthermore, the Brønsted acid density of H-DNL-6 is determined by

Table 4
Steady-state conversion and product selectivity in the methanol amination reaction on DNL-6 [a].

Sample	Reaction temperature (°C)	CH_3OH conversion (%)	Selectivity [b] (%)					
			CH_4	DME	MMA	DMA	TMA	MMA+DMA [c]
H-DNL-6	260	49.68	0.52	16.60	42.08	36.20	4.60	94.45
	300	88.32	0.19	15.33	26.09	45.93	12.46	85.26
M-DNL-6	260	33.26	0.61	6.16	41.92	41.77	9.54	89.77
	300	79.99	0.20	7.21	24.44	50.69	17.47	81.13
L-DNL-6	260	35.52	0.56	7.71	36.35	33.03	22.36	75.63
	300	82.86	0.27	10.49	21.29	31.85	36.11	59.54
SAPO-34 [d]	380	82.00	0.20	3.84	26.78	54.73	14.46	84.94

[a] WHSV = 0.8131 h^{-1}, NH_3/CH_3OH = 2.0, TOS = 146 min. [b] MMA, DMA, and TMA refer to monomethylamine, dimethylamine, and trimethylamine, respectively. Dimethyl ether is considered as a methanol resource. [c] (MMA + DMA) selectivity in the three methylamine products. [d] Sourced from our previous work [34].

^{1}H MAS NMR and a value of 0.69 mmol/g is obtained. This value amounts to 67% of the total acid concentration (1.03 mmol/g), as determined by NH_3-TPD (NH_3 desorption between 325–600 °C), implying the existence of Lewis acid sites with strong acidity in H-DNL-6. This result is indeed consistent with our previous work on the acidity of DNL-6 with a composition of $Si_{0.182}Al_{0.490}P_{0.328}O_2$ [21]. The generation of Lewis acid sites in the structure is a result of the dehydroxylation of adjacent Brønsted acid sites during the calcination process. Herein, considering that amorphous acidic oxides (Al_2O_3 or SiO_2-Al_2O_3) can act as effective catalysts in the industrial methanol amination process, we speculate that the Lewis acid sites in DNL-6 may also contribute to the reaction. For comparison, the results of methanol amination reaction on high-Si SAPO-34 from our previous report [34] are also listed in Table 4. High-Si SAPO-34 contains a larger number of acid sites, but has a lower acid strength than H-DNL-6; the position of the high-temperature NH_3 desorption peak in the NH_3-TPD profile of SAPO-34 was located at 460 °C, whereas it was located at 492 °C for H-DNL-6. From Table 4, it can be understood that a comparable methanol conversion (82%) can only be achieved at a high reaction temperature of 380 °C when SAPO-34 was used as the catalyst. This confirms the effect of acid strength on the methanol amination reaction activity.

H-DNL-6 exhibits a high selectivity for MMA plus DMA. This may be related to the extremely high Si enrichment at the outer shell of H-DNL-6 crystals, which causes a relatively low density of strong acid sites. Therefore, for the product molecules, the probability of consecutive reaction with methanol is reduced when they diffuse out of the inner region to reach the outer surface of the crystals.

4. Conclusions

DNL-6 was hydrothermally synthesized using *N,N'*-dimethylethylenediamine as a novel structure-directing agent. It is found that the crystalline region of the resultant DNL-6 products is wider than previously reported. About 4.4 amines are confined in one α-cage, which implies that more than 8 positive charges can exist simultaneously in one cage to balance the negative charge framework caused by Si incorporation; this explains the relatively high Si content of DNL-6. DNL-6 with an ultrahigh silica content (36.4% Si per mole) shows a remarkable catalytic performance for the methanol amination reaction with a high methanol conversion (>88%) and good selectivity for MMA plus DMA (>85%), implying that DNL-6 is a promising candidate for the synthesis of methylamines.

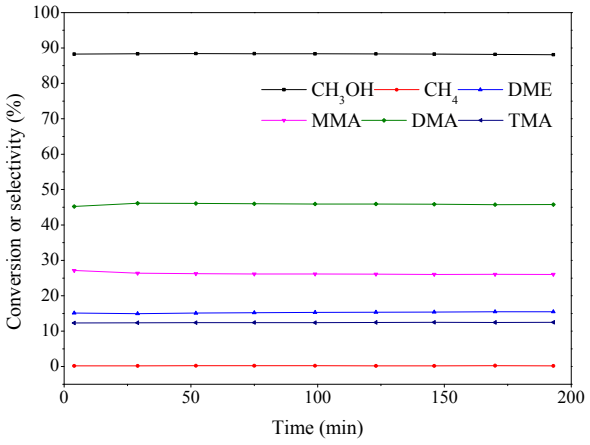

Fig. 8. Methanol conversion and product selectivity in the methanol amination reaction on H-DNL-6 at 300 °C (NH_3/CH_3OH molar ratio = 2/1 and methanol WHSV = 0.813 h^{-1}).

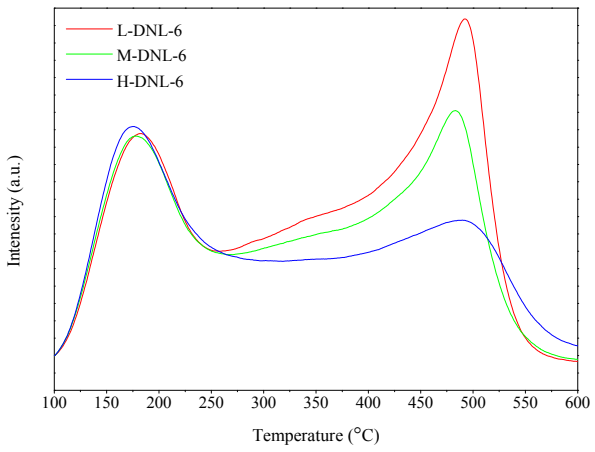

Fig. 9. NH_3-TPD profiles of DNL-6 samples.

Graphical Abstract

Chin. J. Catal., 2018, 39: 1511–1519 doi: 10.1016/S1872-2067(18)63122-5

Silicoaluminophosphate molecular sieve DNL-6: Synthesis with a novel template, *N,N'*-dimethylethylenediamine, and its catalytic application

Pengfei Wu, Miao Yang, Wenna Zhang, Shu Zeng, Mingbin Gao, Shutao Xu, Peng Tian *, Zhongmin Liu *
Dalian Institute of Chemical Physics, Chinese Academy of Sciences; University of Chinese Academy of Sciences

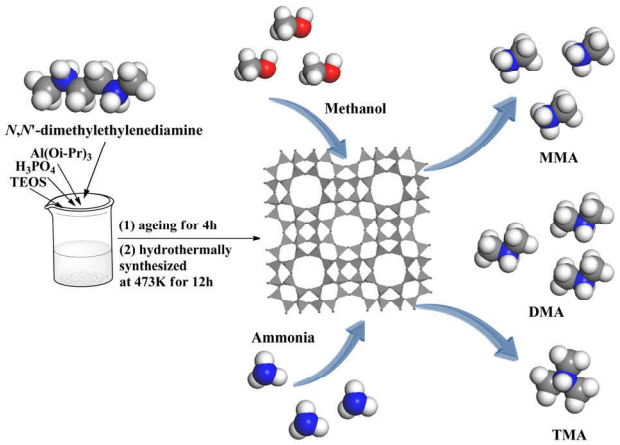

N,N'-dimethylethylenediamine was used as a template to synthesize DNL-6 with a high Si content, which showed excellent catalytic performance in the methanol amination reaction.

References

[1] M. Moliner, C. Martínez, A. Corma, *Chem. Mater.*, **2014**, 26, 246–258.
[2] M. A. Carreon, S. Li, J. L. Falconer, R. D. Noble, *J. Am. Chem. Soc.*, **2008**, 130, 5412–5413.
[3] B. M. Lok, C. A. Messina, R. L. Patton, R. T. Gajek, T. R. Cannan, E. M. Flanigen, *J. Am. Chem. Soc.*, **1984**, 106, 6092–6093.
[4] R. Yadav, A. Sakthivel, *Appl. Catal. A*, **2014**, 481, 143–160.
[5] P. Tian, Y. X. Wei, M. Ye, Z. M. Liu, *ACS Catal.*, **2015**, 5, 1922–1938.
[6] Z. B. Li, J. Martinez-Triguero, P. Concepcion, J. H. Yu, A. Corma, *Phys. Chem. Chem. Phys.*, **2013**, 15, 14670–14680.
[7] D. W. Fickel, E. D'Addio, J. A. Lauterbach, R. F. Lobo, *Appl. Catal. B*, **2011**, 102, 441–448.
[8] J. J. Xue, X. Q. Wang, G. S. Qi, J. Wang, M. Q. Shen, W. Li, *J. Catal.*, **2013**, 297, 56–64.
[9] T. Blasco, A. Chica, A. Corma, W. J. Murphy, J. Agundezrodriguez, J. Perezpariente, *J. Catal.*, **2006**, 242, 153–161.
[10] M. Y. Kim, K. Lee, M. Choi, *J. Catal.*, **2014**, 319, 232–238.
[11] C. S. Cundy, P. A. Cox, *Microporous Mesoporous Mater.*, **2005**, 82, 1–78.
[12] J. W. Zhong, J. F. Han, Y. X. Wei, P. Tian, X. W. Guo, C. S. Song, Z. M. Liu, *Catal. Sci. Technol.*, **2017**, 7, 4905–4923.
[13] Q. M. Sun, Z. K. Xie, J. H. Yu, *Natl. Sci. Rev.*, **2017**, nwx103-nwx103.
[14] P. F. Wu, M. Yang, W. N. Zhang, S. T. Xu, P. Guo, P. Tian, Z. M. Liu, *Chem Commun.*, **2017**, 53, 4985–4988.
[15] H. van Heyden, S. Mintova, T. Bein, *Chem. Mater.*, **2008**, 20, 2956–2963.
[16] Z. B. Li, J. Martínez-Triguero, J. H. Yu, A. Corma, *J. Catal.*, **2015**, 329, 379–388.
[17] P. Tian, X. Su, Y. X. Wang, Q. H. Xia, Y. Zhang, D. Fan, S. H. Meng, Z. M. Liu, *Chem. Mater.*, **2011**, 23, 1406–1413.
[18] X. Su, P. Tian, J. Z. Li, Y. Zhang, S. H. Meng, Y. L. He, D. Fan, Z. M. Liu, *Microporous Mesoporous Mater.*, **2011**, 144, 113–119.
[19] X. Su, P. Tian, D. Fan, Q. H. Xia, Y. Yang, S. T. Xu, L. Zhang, Y. Zhang, D. H. Wang, Z. M. Liu, *ChemSusChem*, **2013**, 6, 911–918.
[20] D. Fan, P. Tian, S. T. Xu, Q. H. Xia, X. Su, L. Zhang, Y. Zhang, Y. L. He, Z. M. Liu, *J. Mater. Chem.*, **2012**, 22, 6568–6574.
[21] X. Su, S. T. Xu, P. Tian, J. Z. Li, A. M. Zheng, Q. Wang, M. Yang, Y. X. Wei, F. Deng, Z. M. Liu, *J. Phys. Chem. C*, **2015**, 119, 2589–2596.
[22] J. Z. Li, Y. X. Wei, J. R. Chen, P. Tian, X. Su, S. T. Xu, Y. Qi, Q. Y. Wang, Y. Zhou, Y. L. He, Z. M. Liu, *J. Am. Chem. Soc.*, **2012**, 134, 836–839.
[23] M. Yang, P. Tian, L. Liu, C. Wang, S. T. Xu, Y. L. He, Z. M. Liu, *CrystEngComm*, **2015**, 17, 8555–8561.
[24] J. A. van Bokhoven, D. C. Koningsberger, P. Kunkeler, H. van Bekkum, A. P. M. Kentgens, *J. Am. Chem. Soc.*, **2000**, 122, 12842–12847.
[25] T. Takewaki, L. W. Beck, M. E. Davis, *Microporous Mesoporous Mater.*, **1999**, 33, 197–207.
[26] M. E. Davis, C. Saldarriaga, *J. Chem. Soc., Chem. Commun.*, **1988**, 920–921.
[27] P. Tian, B. Li, S. T. Xu, X. Su, D. H. Wang, L. Zhang, D. Fan, Y. Qi, Z. M. Liu, *J. Phys. Chem. C*, **2013**, 117, 4048–4056.
[28] L. Frydman, J. S. Harwood, *J. Am. Chem. Soc.*, **1995**, 117, 5367–5368.
[29] W. L. Shen, X. Li, Y. X. Wei, P. Tian, F. Deng, X. W. Han, X. H. Bao, *Microporous Mesoporous Mater.*, **2012**, 158, 19–25.
[30] D. Fan, P. Tian, S. T. Xu, D. H. Wang, Y. Yang, J. Z. Li, Q. Y. Wang, M. Yang, Z. M. Liu, *New J. Chem.*, **2016**, 40, 4236–4244.

[31] D. R. Corbin, S. Schwarz, G. C. Sonnichsen, *Catal. Today*, **1997**, 37, 71–102.
[32] B. Tijsebaert, B. Yilmaz, U. Müller, H. Gies, W. P. Zhang, X. H. Bao, F. S. Xiao, T. Tatsumi, D. De Vos, *J. Catal.*, **2011**, 278, 246–252.
[33] H. Y. Jeon, C. H. Shin, H. J. Jung, S. B. Hong, *Appl. Catal. A*, **2006**, 305, 70–78.
[34] Y. Y. Qiao, P. F. Wu, X. Xiang, M. Yang, Q. Y. Wang, P. Tian, Z. M. Liu, *Chin. J. Catal.*, **2017**, 38, 574–582.

以*N*,*N*'-二甲基乙二胺为模板剂合成磷酸硅铝分子筛DNL-6及其在催化中的应用

吴鹏飞[a,b], 杨 淼[a], 张雯娜[a,b], 曾 姝[a,b], 高铭滨[a,b], 徐舒涛[a], 田 鹏[a,*], 刘中民[a,#]
[a]中国科学院大连化学物理研究所, 甲醇制烯烃国家工程实验室, 辽宁大连116023
[b]中国科学院大学, 北京100049

摘要: 磷酸硅铝类分子筛由于其温和的酸性以及良好的热稳定性和水热稳定性在催化领域得到了广泛的应用. 例如SAPO-34分子筛具有优异的催化甲醇制烯烃反应的催化活性, 经过铜离子交换后的Cu-SAPO-34分子筛在选择性催化还原NO_x过程中体现了良好的活性及稳定性. 在磷酸硅铝分子筛的合成过程中往往需要使用有机胺或铵盐作为有机结构导向剂. 导向剂起到了溶解原料、导向结构、匹配电荷、填充骨架空间等复杂的作用, 因此开发新型的有机结构导向剂是调节磷酸硅铝分子筛晶相、形貌以及酸性位点分布的最重要的手段. DNL-6分子筛是由本课题组首次报道的具有RHO拓扑结构的磷酸硅铝分子筛, 由于其丰富的酸位点以及适宜的孔口尺寸在CO_2/CH_4和CO_2/N_2吸附分离过程中体现出良好的应用前景. 此外由于DNL-6分子筛具有非常强的酸性(接近H-ZSM-5), 在DNL-6分子筛上首次发现MTO反应过程中的活性中间体七甲基苯基碳正离子. 截止目前为止二乙胺是唯一被报道的成功导向DNL-6分子筛的有机胺模板剂, 在水热合成过程中必须使用阳离子表面活性剂以防止DNL-6分子筛的溶解与转晶, 同时产品的组成调节困难。

本论文主要报道了一种新型的有机胺模板剂*N*,*N*'-二甲基乙二胺在水热条件下成功导向具有很高的结晶度与较高的硅含量范围(20%–35%)的DNL-6分子筛, 对DNL-6产物进行X射线衍射、X射线荧光分析、X射线光电子能谱、扫描电镜以及氮气物理吸附等一系列系统表征. 热重分析表明DNL-6分子筛α笼中较大的模板剂容纳量(单位α笼中容纳4.4个模板剂分子)是成功得到具有超高硅DNL-6分子筛(硅摩尔含量达36.4%)的原因. 结合固体魔角旋转核磁(^{13}C, ^{29}Si, ^{27}Al, ^{31}P以及多量子^{27}Al)对分子筛骨架的原子配位环境的分析以及XPS表征表明超高硅DNL-6分子筛具有复杂的硅环境分布, 晶粒外表面以酸密度很低的大面积硅岛为主, 沿晶粒半径方向向晶体内部硅含量逐渐下降同时硅岛面积逐渐减小, 晶粒中心的硅环境主要以Si(4Al)为主. 由于超高硅DNL-6分子筛较强的酸强度、合适的酸位点分布以及狭窄的孔道尺寸在甲醇氨化反应中得到了超过88%的甲醇转化率以及85%的甲胺+二甲胺选择性.

关键词: *N*,*N*'-二甲基乙二胺; 磷酸硅铝分子筛; 合成; DNL-6; 甲醇氨甲基化反应

收稿日期: 2018-05-07. 接受日期: 2018-06-02. 出版日期: 2018-09-05.
*通讯联系人. 电话: (0411)84379218; 传真: (0411)84691570; 电子信箱: tianpeng@dicp.ac.cn
#通讯联系人. 电话: (0411)84379998; 传真: (0411)84691570; 电子信箱: liuzm@dicp.ac.cn
基金来源: 国家自然科学基金(21476228, 21676262); 中国科学院前沿科学重点研究项目(QYZDB-SSW-JSC040).
本文的电子版全文由Elsevier出版社在ScienceDirect上出版(http://www.sciencedirect.com/science/journal/18722067).